Control System of Ocean Wave Simulator Using PID-Salp Swarm Algorithm

Affiani Machmudah[1], Juchen Li[2], Mahmud Iwan Solihin[3], Chiong Meng Choung[4],
Wibowo Harso Nugroho[5], Ahmad Syafiul Mujahid[6], Sahlan[7], Abdul Ghofur[8]
Research Center for Satellite Technology, National Research and Innovation Agency (BRIN), Bogor, Indonesia[1]
Faculty of Engineering-Technology and Built Environment, UCSI University, Kuala Lumpur, Malaysia[2, 3, 4]
School of Intelligent Manufacturing, Anhui Wenda University of Information Engineering, Hefei, China[2]
Research Center for Hydrodynamics Technology, National Research and Innovation Agency (BRIN), Surabaya, Indonesia[5, 6, 7, 8]

***Abstract*—This paper presents a control system optimization of an ocean wave simulator using a meta-heuristic optimization. The proposed control system involves finding leg length trajectories by an Inverse Kinematics (IK) to be used as references for a Proportional-Integral-Derivative (PID). PID gains are tuned using a Salp Swarm Algorithm (SSA) with a Root Mean Square Error (RMSE) of leg position errors as a performance index. A Stewart platform dynamic is modeled in Simscape Multibody, integrated with a trajectory generator, an IK module, and a control system diagram block in Simulink models. The Simulink model of Stewart platform dynamics is then called in the optimization procedure by writing the programming code in MATLAB. Results show that the SSA outperforms other meta-heuristic methods, namely a Genetic Algorithm (GA) and a Particle Swarm Optimization (PSO), achieving the lowest fitness value, 16.8% and 8.7% lower than GA and PSO, respectively. Moreover, the SSA avoids boundary-trapping issues encountered by the PSO, which is stuck at its upper bound. The SSA has successfully enhanced the simplified version of the PID control system, where the scenario of the simplified PID-SSA scenario achieves better tracking error performance than the full PID-SSA configuration. The proposed approach contributes to the advancement of marine simulation technologies, supporting innovation in ocean engineering and sustainable maritime applications.**

Keywords*—Marine simulation technologies, Stewart platform; ocean wave; control system; meta-heuristic optimization; Salp Swarm Algorithm

I. Introduction

The ocean is a vital part of the Earth and plays a significant role in the global ecosystem. Since approximately 70% of the Earth's surface is covered by ocean, conducting research in the maritime field is essential. One key challenge in this area is managing and understanding ocean waves. However, testing newly developed marine technologies directly in the real ocean is often difficult and costly, especially due to the complexity of transporting and deploying such systems. As a result, modeling and simulation have become crucial areas of maritime research. Simulation technologies can replicate real ocean conditions, allowing researchers to observe and analyze the performance of the developed systems effectively.

Generally, there are two types of ocean wave simulators: simulation platforms and ocean engineering basins [1]. A simulation platform applies wave models to control a motion platform, while an ocean engineering basin uses known ocean wave models as input for controlling a wave-making system. One of the most widely used simulation platforms for ocean wave simulation is the Stewart platform. The Stewart platform has been extensively utilized in the development and testing of ocean technology applications ranging from ship motion simulation [1-5], harbor crane robotics technologies [6-8], to ocean wave compensators [9-13].

The Stewart platform is a parallel manipulator that has superiorities in accuracy, rigidity, and capability in carrying heavy loads that to the series manipulator. Controlling the parallel manipulator is difficult due to its complex, coupled nonlinear dynamics, demanding advanced methods for reliable performance. As the Stewart platform is expected to execute complex motions with stability, its control systems remain a critical area of research. Silva *et al*. [14] employed the industrial controller on the Stewart platform, addressing kinematics and motion automation. The IK considered two scenarios: point-to-point cycloidal trajectories and oceanic wave motion. Vu *et al*. [15] presented a distributed control technique based on finite-time distributed sliding mode control. Each leg of the Stewart platform was considered as an autonomous agent. The dynamic of the Stewart platform was modeled using a Lagrangian-based approach. The trajectory tracking control by the Stewart platform using a PD+ controller was presented by Tamir *et al*. [16]. The dynamic of the Stewart platform was modelled using the Euler-Lagrange method. The motion was simulated using MATLAB/Simulink and validated using ADAM software. Lin *et al*. [17] presented drag-free control of the Stewart platform for satellite ground simulation. Inverse Kinematics (IK) and dynamics of the Stewart platform based on Newton-Euler were employed. Two degree-of-freedom drag-free controller was proposed using an algorithm of H_∞ loop shaping. An adaptive control of the pneumatic actuator of the sixth degree-of-freedom Stewart platform was presented by Andrievsky *et al*. [18]. Pneumatic valve groups and a spool valve were involved. Control process, discretization, and pneumatic drive load changes were considered.

Artificial Intelligent methods such as meta-heuristic optimization and an Artificial Neural Network (ANN) have been employed in the control system of the Stewart platform. Barghandan *et al*. [19] proposed a sliding mode control based on the Genetic Algorithm (GA) considering uncertainties and

external disturbances. An adaptation law based on a barrier function had removed the requirement of the external disturbance upper bounds. Tamir *et al*. [20] presented an extended Proportional-Derivative (PD) sliding mode controller for the Stewart platform trajectory tracking. Gain tuning was performed using modified grey wolf optimization with integral absolute error as a cost function. Validation was performed using the ADAM software. Sumnu *et al*. [21] presented the Proportional-Integral-Derivative (PID) control system of the Stewart manipulator, where the linear motor transfer function is derived and modeled in Simulink block diagram. The effect of the inertia of the lower legs on the dynamic performance was studied. Velasco *et al*. [22] presented the ANN to improve the accuracy of the Stewart platform when it holds a camera. The ANN model was designed based on the kinematics and dynamics analysis. Based on the inverse ANN model and additional integral control, the control system was then developed. Du *et al*. [13] applied the Stewart platform as a marine stabilized platform and proposed an extended state observer-based sliding mode control (ESO-SMC) to enhance the stability and anti-disturbance of the hydraulic actuator on the system platform. Kinematic and dynamic models were analyzed first, and the Marine Predator Algorithm (MPA) was applied to optimize the ESO-SMC. Simulation was conducted in MATLAB in Simulink using models of an engineering ship and a marine stabilized platform, which was placed on top of the ship model. An *et al*. [23] designed a Fracture Reduction Robot (FRR) based on the Stewart platform as an orthopedic surgery robot. A sparrow search algorithm was applied to tune the controller gains of the FRR. The IK was used, and the FRR dynamics were modeled in Simulink. The mechanism of fracture reduction was proposed using computer torque control.

The paper is organized as follows: Section II presents the kinematics and dynamics of a 6-DOF Stewart platform-based ocean wave simulator. Section III describes the motion simulator system. The trajectories generation, the control system optimization, and the Salp Swarm Algorithm (SSA) are presented in Section IV. Results and discussions are presented in Sections V and VI, respectively. Conclusions are presented in Section VII.

II. Kinematics and Dynamics

Kinematics and dynamics analysis are necessary for controlling the Stewart platform-based ocean wave simulator. For the dynamics analysis, this paper models the Stewart platform using Simscape Multibody to be optimized by the SSA via MATLAB and Simulink environments. MATLAB and Simulink have been used to model complex dynamical systems, including the Stewart platform to analyze the proposed methods before implementing them in the real system.

A. Inverse Kinematics

There are two kinds of kinematics problems for Stewart platform motion, namely Inverse kinematics (IK) and Forward Kinematics (FK). The FK is the problem of finding the positions and orientations of payload platform when leg lengths are defined while the IK is the problem of finding the leg lengths of Stewart platform when positions and orientations of payload platform are known. This paper considers tracking the prescribed paths, which are the ocean wave model so that using the 6-DOF Stewart platform, converting the tracking paths to the leg lengths trajectories is necessary to be done via an IK computation. Fig. 1 illustrates the coordinates assigned for the Stewart platform. There is a base platform coordinate {B} located at the center of the base table and a payload platform coordinate {P} located at the center of the payload table.

A closed-form IK solution can be obtained using geometrical and algebraic analysis as follows [24]:

$$l_i^2 = x^2 + y^2 + z^2 + r_P^2 + r_B^2 + 2\left(r_{11}P_{ix} + r_{12}P_{iy}\right)(x - b_{ix}) + 2\left(r_{21}P_{ix} + r_{22}P_{iy}\right)\left(y - b_{iy}\right) + 2\left(r_{31}P_{ix} + r_{32}P_{iy}\right)z - 2\left(xb_{ix} - yb_{iy}\right) \quad (1)$$

The above equation needs the orientation matrix. The orientation of the Roll-Pitch-Yaw angle is expressed as follows:

$$R_{RPY} = \begin{bmatrix} c\alpha\, c\beta & c\alpha\, s\beta\, s\gamma - s\alpha\, c\gamma & c\alpha\, s\beta\, c\gamma - s\alpha\, s\gamma \\ s\alpha\, c\beta & s\alpha\, s\beta\, s\gamma - c\alpha\, c\gamma & s\alpha\, s\beta\, c\gamma - c\alpha\, s\gamma \\ -s\beta & c\beta\, s\gamma & c\beta\, c\gamma \end{bmatrix} \quad (2)$$

where, R_{RPY}, α, β, γ, s, and c are the orientation matrix, roll angle, pitch angle, yaw angle, sinus, and cosinus, respectively.

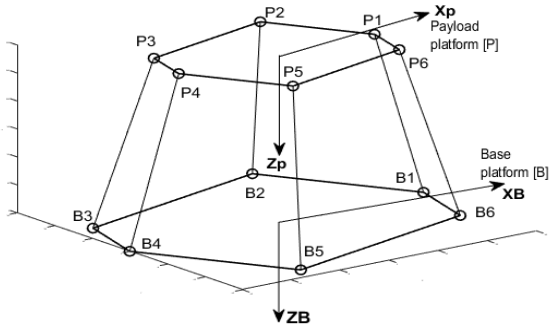

Fig. 1. Frame coordinate of the Stewart platform.

B. Dynamics

Dynamics of the Stewart platform can be expressed in the following form [25]:

$$F = M(q)\ddot{q} + N(q, \dot{q}) + G(q) \quad (3)$$

where, $M(q)$ is the inertia matrix, $N(q, \dot{q})$ is components of Coriolis and centrifugal force, $G(q)$ is the components of gravity force.

The inverse dynamics is the problem of finding the force/torque for known positions, velocities, and accelerations for defined positions, velocities, and acceleration vectors. This paper employs Simscape Multibody for solving the forward dynamics of the Stewart platform in the control system. Detail of the Simscape block diagram is shown in Fig. 2.

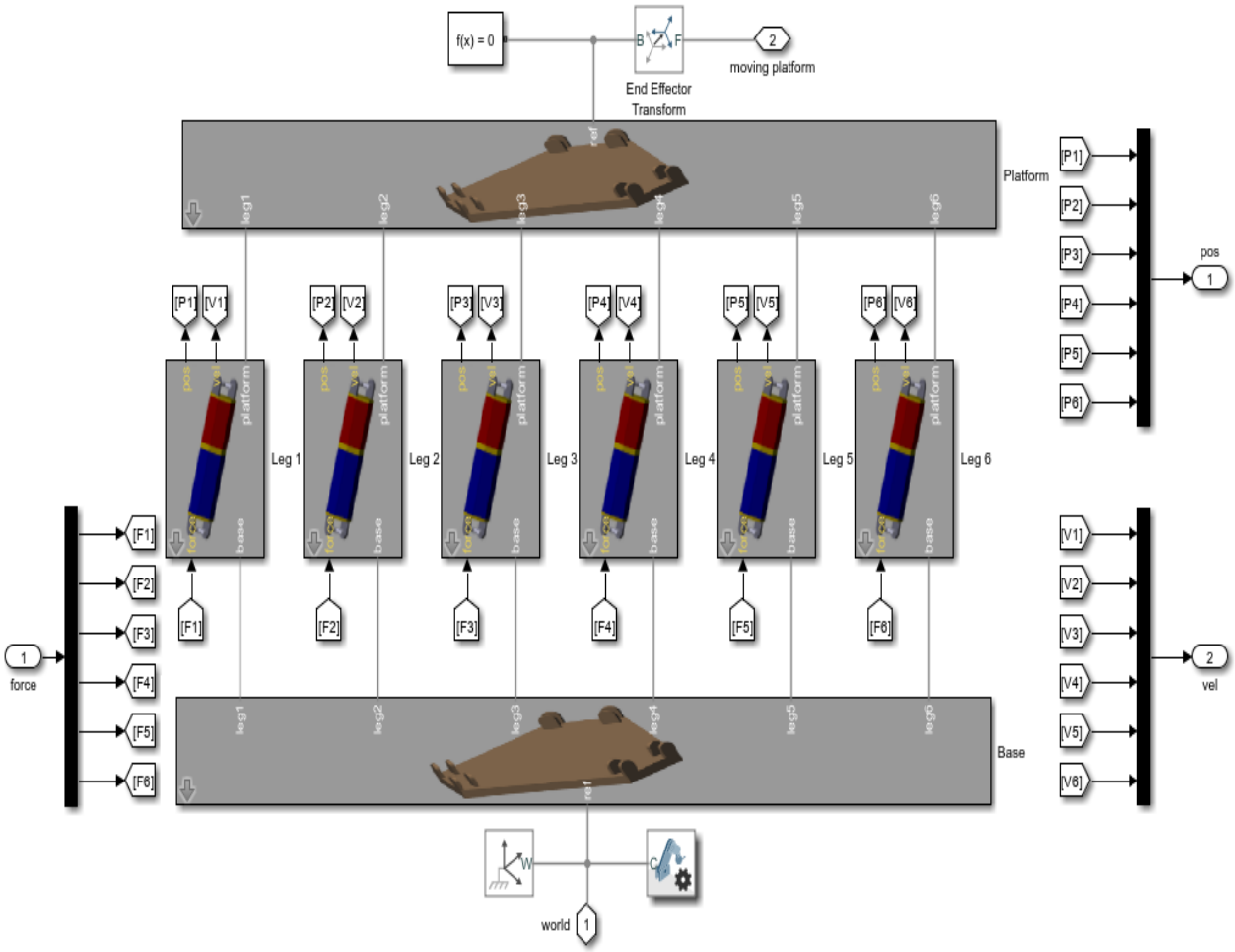

Fig. 2. Dynamic modeling of the Stewart platform using Simulink Multibody.

III. Motion Simulator System

Fig. 3 illustrates the ocean wave simulator system. The traced path is generated by the trajectory generator. An IK module processes the data from the trajectory generator to obtain the requested leg positions, which become the input for the control system of the Stewart platform.

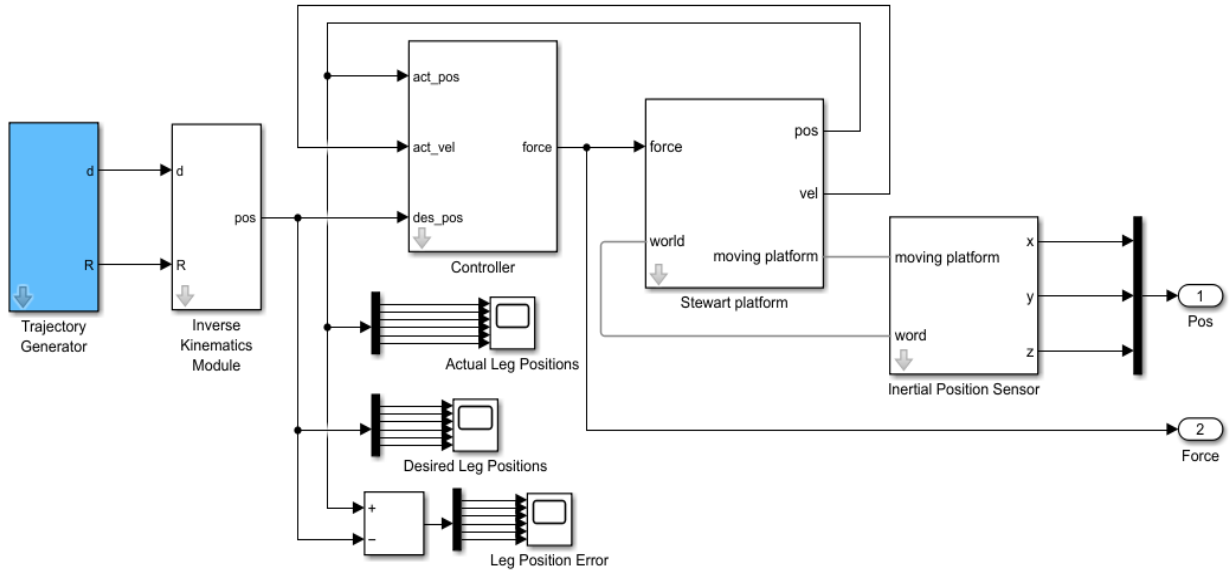

Fig. 3. Ocean wave simulator system.

A. Trajectory Generations

Ocean wave models used in this paper is presented in Table I. They are the modification of ocean wave models presented in [1]. This modification is necessary because the parameter of the Stewart platform is different and the Stewart platform has the workspace which depends on the parameter of the Stewart platform.

TABLE I. OCEAN WAVE MODELS [1]

Motion forms	Model (cm)
Lateral	$8\sin(0.25\pi t)$
Transverse	$8\sin(0.25\pi t)$
Lifting	$8\sin(0.25\pi t)$
Rolling	$\frac{10\pi}{180}\sin(0.25\pi t)$
Pitching	$\frac{8\pi}{180}\sin(0.25\pi t)$

IV. CONTROL SYSTEM OPTIMIZATIONS

Fig. 5 illustrates the algorithm of the control system optimization. Ocean wave models need to be converted to leg length trajectories via the IK. These leg length trajectories become the reference trajectories that need to be tracked by the control system of the motion simulator. This paper uses the PID-based control system to be optimized by the SSA. A comprehensive computation is necessary through integration of MATLAB software, Simulink, and Simscape Multibody. The responses of the Stewart platform are obtained using the Simulink to examine the Simscape Multibody modeling of Stewart platform.

Fig. 4 shows the block diagram of the ocean wave model represented in Table I. The Stewart platform uses in this paper has parameter as presented in Tabel II.

Finding the optimal gains by meta-heuristic optimization are performed by writing the code in m-file, MATLAB. Using the IK presented in the previous section, the trajectories of leg lengths can be obtained. These leg lengths trajectories should be within the Δl_{max} boundary. In the case the leg length trajectories are outside the boundary, the initial condition, which is the initial distance between the fixed base and moving base H, possibly needs to be recalculated. The Δl_{max} can be obtained by the geometric analysis of the Stewart platform.

A. PID Control System

Leg lengths trajectories from the trajectories generator become the reference signal of the control system. This paper uses the conventional PID control system optimized by the SSA. The detail of the simplified PID control system as the Simulink block diagram is illustrated in Fig. 6.

TABLE II. STEWART PLATFORM PARAMETER

Parameters	Values
Radius of moving platform (hexagon)	18 cm
Radius of fixed platform (hexagon)	28 cm
Cylinder radius of leg	3 cm
Maximum upper leg length	10 cm
Maximum lower leg length	30 cm
Initial distance between the fixed base and moving platform, H	13.5 cm

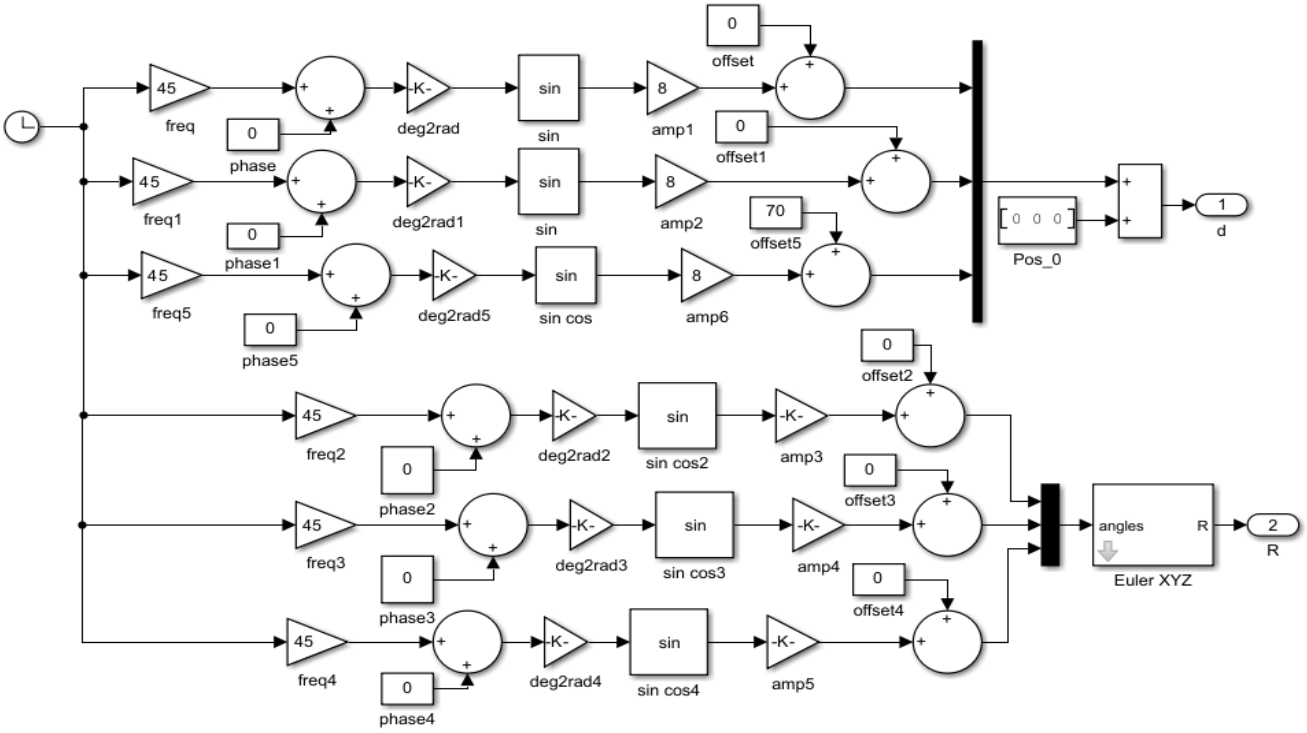

Fig. 4. Diagram block of trajectory generation of ocean wave motion.

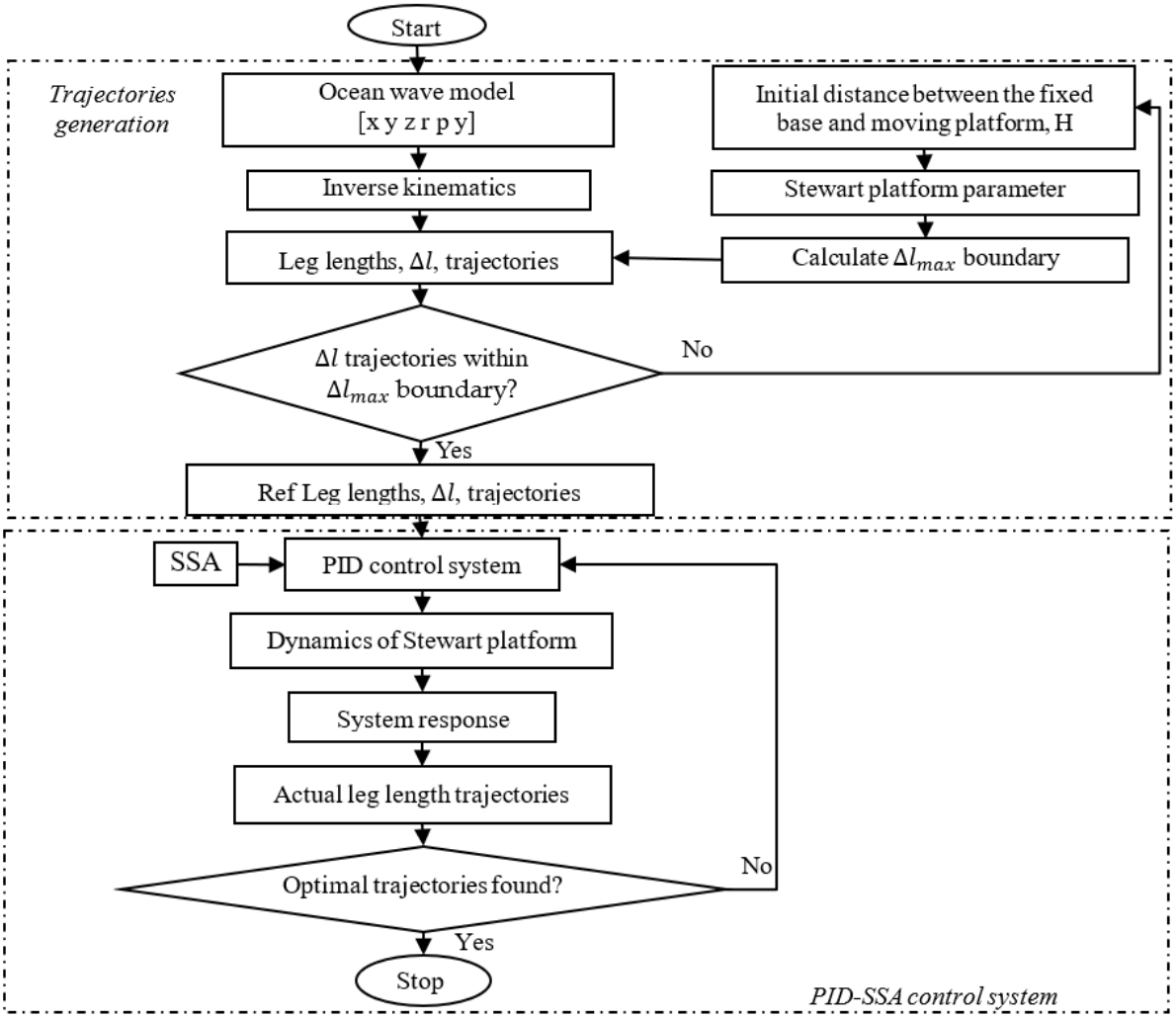

Fig. 5. Control system algorithm of the Stewart platform.

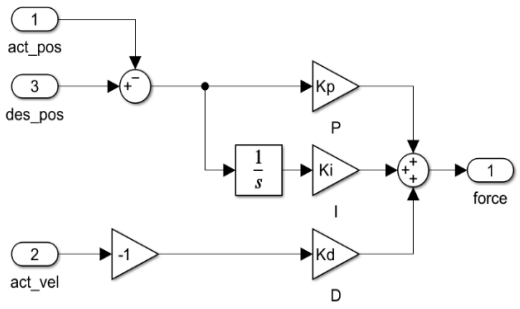

Fig. 6. Simplified conventional PID control system block diagram.

The simplified conventional PID control law is employed as follows:

$$F = K_p e + K_i \varepsilon - K_d \dot{\Delta l} \tag{4}$$

$$e = \left(\Delta l_{ref} - \Delta l\right) ; \dot{\varepsilon} = e$$

where, F, e, Δl, Δl_{ref}, $\dot{\Delta l}$, K_p, K_i, and K_d are force feedback control, error leg length, actual leg length, desired leg length, actual leg velocities or first derivative of Δl, proportional gain, integral gain, and derivative gain, respectively.

B. Salp Swarm Algorithm

The PID gains are optimized by the SSA with the objective optimization is to minimize the Root Mean Square Error (RMSE) as the cost function. The SSA is relatively new meta-heuristic optimization proposed in 2017 by Mirjalili *et al.* [26]. The SSA is inspired by the salps swarming behaviour when they are navigating and foraging in deep oceans.

The populations consists two groups, namely leader and followers. The leader is the salp at the chain front. The leader position is updated as follows:

$$x_j^1 = \begin{cases} F_j + c_1\left(\left(ub_j - lb_j\right)c_2 + lb_j\right) & c_3 \geq 0 \\ F_j - c_1\left(\left(ub_j - lb_j\right)c_2 + lb_j\right) & c_3 < 0 \end{cases} \tag{5}$$

where, x_j^1, F_j, ub_j, and lb_j, are the leader position in jth dimension, the food source in jth dimension, upper bound in jth dimension, lower bound in jth dimension, respectively. Parameters c_1, c_2, and c_3 are random numbers.

Above leader position is updated based on the food source. For exploration and exploitation, the following parameter is defined:

$$c_1 = 2e^{-\left(\frac{4l}{L}\right)^2} \quad (6)$$

where, l and L is the current iteration and the maximum iteration number, respectively. The c_2, and c_3 parameters are generated randomly in interval [0, 1].

The follower position is updated as follows:

$$x_j^i = \frac{1}{2}\left(x_j^i - x_j^{i-1}\right) \quad (7)$$

where, $i \geq 2$ and x_j^i is the ith follower salp position in jth dimension.

V. Results

Besides the SSA, other meta-heuristic optimizations, which are the Genetic Algorithm (GA) and Particle Swarm Optimization (PSO), are also executed as comparison methods. The GA, PSO, and SSA use 10 individuals in the population evaluated for 50 iterations. The optimization parameters are searched within the search area [100, 10000] for K_p gain and [2, 1000] for the K_i and K_d gains. The result of Δl_{max} is 30 cm for the Stewart platform used in this paper (Table II). The computation of the gain optimization is performed within 2.5 seconds and divides the motion into 200 sampling times.

Fig. 7 shows the results of the leg length trajectories using the IK for the value of H = 13.5 cm. It can be observed that the leg lengths trajectories are within their workspace, where all trajectories are within Δl_{max} boundary.

A. Trial-and-Error Gains

It is generally known that tuning the PID gain is a challenging computational problem, while using a trial-and-error approach is a tedious task. The fitness value using this gain is 6.642 for the trial-and-error gain, [K_p K_i K_d] = [300 100 100]. Fig. 8 shows the system response for the trial-and-error gains. The difference between the desired trajectories and the actual trajectories is not small, so tuning the gains is necessary to obtain the efficient motion.

B. Optimal Gains

Results of the optimal gains by the GA, PSO, and SSA are presented in Table III. The computation of the RMSE as the fitness function is performed for 2.5 second running time. It shows that the SSA algorithm is outperformed the GA and PSO where the SSA has the lowest fitness value. It can also be observed that the SSA does not trap to the upper bound value and lower bound value.

The SSA has ability to explore and exploit the searching area through parameter c_1 in Eq. (6). On the contrary, the PSO has been trapped to the upper bound value for the K_p (K_p = 10000). Fig. 9 shows the fitness value evolution during 50 numbers iterations. The fitness value of the SSA is 16.8% and 8.7% lower than the GA and the PSO, respectively.

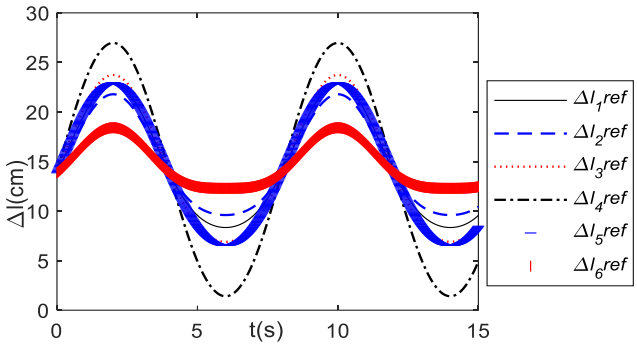

Fig. 7. Leg lengths trajectories of the ocean wave model within Δl_{max} boundary.

TABLE III. Results of GA, PSO, SSA

Methods	Fitness value	Best [K_p K_i K_d]
GA	0.0781	[9661.2 992.4 20]
PSO	0.072	[10000 6190 20]
SSA	*0.066*	[7472.4 747.24 5]

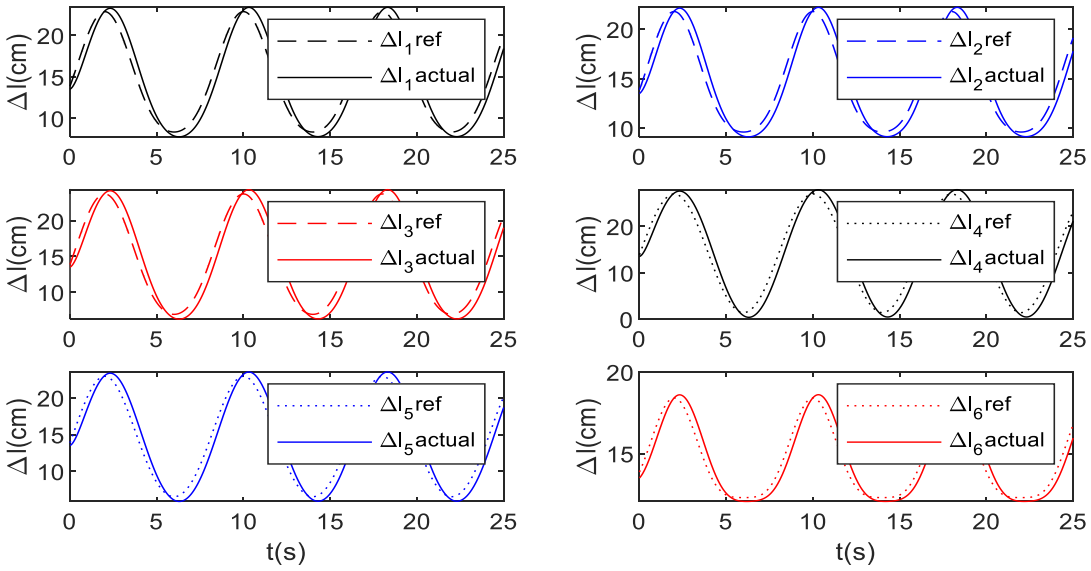

Fig. 8. System response for the trial and error approach [K_p K_i K_d] = [300 100 100].

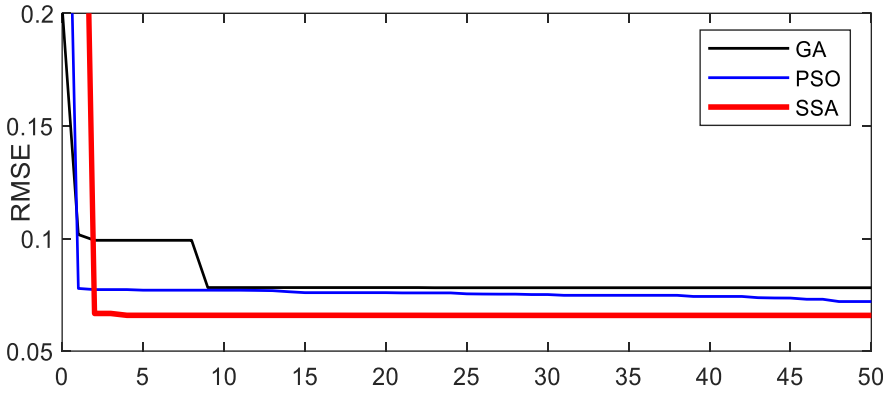

Fig. 9. Fitness value of GA, PSO, and SSA.

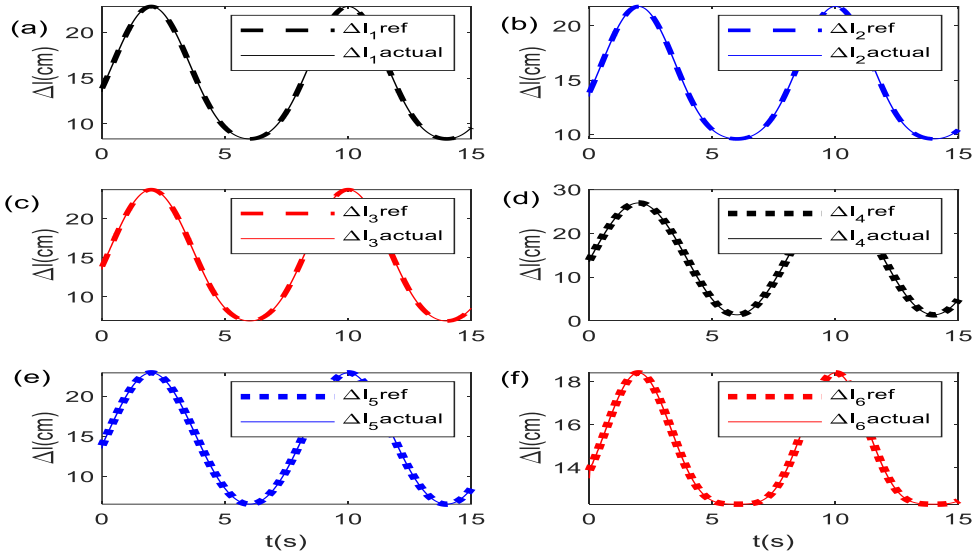

Fig. 10. System response for the SSA method, [K_v K_p K_i] = [7472.4 747.24 5].

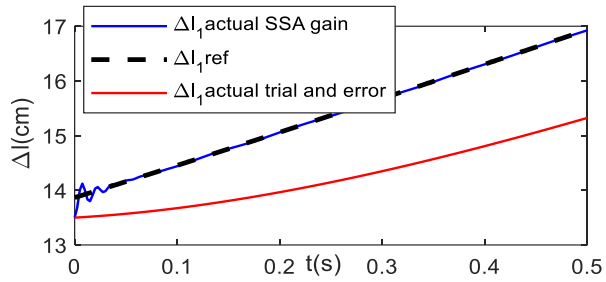

Fig. 11. Zoom in of system response by SSA and trial-and-error gain.

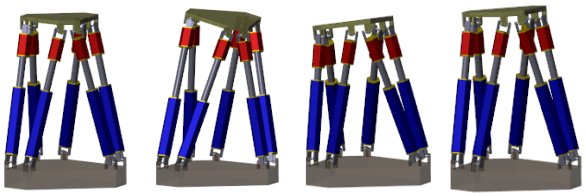

(a) (b) (c) (d)

Fig. 12. Motion frames of the ocean wave simulator K=[7472.4 747.24 5] (a) 0 second (b) 2.5 second (c) 5 second (d) 7.5 second.

Fig. 10 shows the system response of the SSA gains. As compare with the respond from the trial-and-error gain, it can be observed that the SSA has significantly improved the trial-and-error approach. Fig. 11 shows detail of comparison between the results of the SSA gains and the trial and error gains for fist leg length trajectories. Fig. 12 shows the motion frame of the Stewart platform during tracking the ocean wave model.

C. PID with Velocity Reference

The previous result was obtained from the simplified version of the PID control system without feedforward of the velocity setpoint. This section investigates the performance of full PID control system when the velocity reference is included as an input to the controller.

The full version of the PID control law, in which the velocity reference is used as the control input, is expressed as follows:

$$F = K_p e + K_i \varepsilon - K_d \dot{e} \tag{8}$$

$$e = \dot{\Delta l}_{ref} - \dot{\Delta l}$$

The detail of the block the Simulink block diagram is illustrated in Fig. 13.

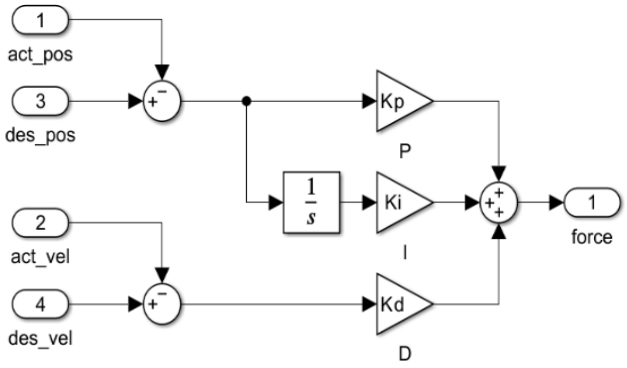

Fig. 13. Full version of PID control system block diagram.

Table IV presents the results of the trial-and-error and SSA gains for the PID control system with velocity reference input. By accommodating the velocity reference in the simplified conventional PID control, using the same trial-and-error gain K = [300 100 100], the fitness value has significantly improved to 0.7450. However, this value is still far from the SSA gain, where the fitness achieved to 0.066 (Table III).

VI. Discussions

The SSA has significantly improved the RMSE of the ocean wave simulator's motion. Fig. 14 presents the detailed system response for the trial-and-error gains of the full version PID control system. However, when the SSA gains from the previous section (see Table III) are applied with the velocity reference included, the resulting fitness value is 0.1052—worse than that of the simplified PID control system.

The performance of the full version of the PID control system is further investigated by tuning the gains using the SSA. Using the same computation parameters as in the simplified PID, the optimization result is presented in Table IV. The SSA gain for the PID control is K = [8148.97 814.9 b37.64] with the fitness value is 0.099443. Based on the fitness value result, the simplified PID-SSA has better performance than that of the PID-SSA.

TABLE IV. Results of SSA for Full Version of the PID System

Methods	Fitness value	$[K_p\ K_i\ K_d]$
Trial-and-error	0.7450	[300 100 100]
Gain from previous section	0.1052	[7472.4 747.24 5]
SSA	0.099443	[8148.97 814.9 37.64]

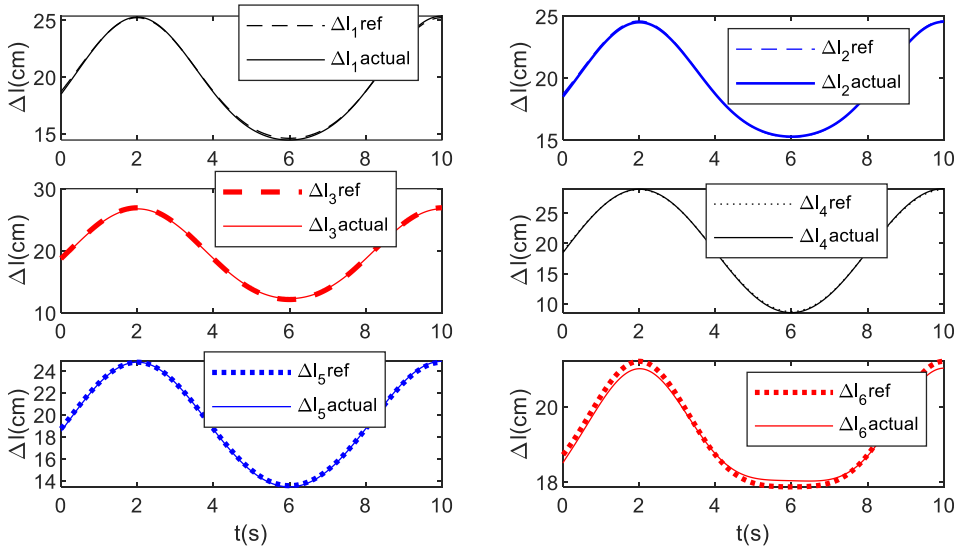

Fig. 14. System response of PID with velocity reference for the trial and error approach, $[K_p\ K_i\ K_d]$ = [300 100 100].

Employing the SSA in the PID control system of the ocean wave simulator has yielded promising results. Adding the velocity reference input into the PID improves the simulator's response for the trial-and-error gain, as reflected in the fitness value results. However, when the SSA is applied to correct the required force, the simplified PID (without the velocity reference input) outperformed the SSA-PID. The main challenge in reducing the position tracking error likely stems from the highly nonlinear dynamics of the 6-DOF Stewart platform. Standard PID control systems often require additional compensation to handle such nonlinearities effectively. Therefore, for future work, incorporating advanced nonlinear compensation methods, such as computed-force control, can be investigated to further enhance the system respond of the PID control system.

VII. Conclusions

The control system optimization of the Stewart-platform-based ocean wave simulator using the PID-SSA method has been presented. The system solved the IK to obtain leg length trajectories, used as reference inputs for the PID controller. By employing Simscape Multibody to handle the forward dynamics, IK module, and PID control, the SSA was applied to tune the PID gains. Results showed that the SSA not only success to identify the optimal gain, but also significantly enhance the performance of the simplified PID controller as

compare to the full version of the PID controller. The promising performance of SSA in improving simplified PID control suggests strong potential for its application to ocean wave compensators in ships and ocean floating platforms. Future work should address nonlinear compensation in simulator dynamics and extend the proposed method to wave-induced motion control on offshore platforms.

ACKNOWLEDGMENT

The research in this article was funded by the Professional Leader Training Program of Anhui Provincial Department of Education (No. DTR2024059). This research was supported by Riset dan Inovasi untuk Indonesia Maju (RIIM) Batch 4 by Lembaga Pengelola Dana Pendidikan (LPDP) (Grant No. 37/II.7/HK/2023).

REFERENCES

[1] W. Chuan, D. Huafeng, and H. Lei, “A dynamic ocean wave simulator based on six-degrees of freedom parallel platform,” Proc Inst Mech Eng C J Mech Eng Sci, vol. 232, no. 20, pp. 3722–3732, Oct. 2018, doi: 10.1177/0954406217739647.

[2] Z. Zhou, B. Zhang, J. Chang, Q. Dong, and H. Wang, “Dynamic response analysis of the vessel under the action of motion compensation equipment,” Ocean Engineering, vol. 315, Jan. 2025, doi: 10.1016/j.oceaneng.2024.119885.

[3] Z. Li, H. Du, J. Si, Z. Wang, and W. Xiong, “Rigid-flexible coupling dynamic modeling and validation of a helicopter rescue simulator based on an inverted Stewart platform,” Ocean Engineering, vol. 319, Mar. 2025, doi: 10.1016/j.oceaneng.2024.120164.

[4] T. Ono, R. Eto, J. Yamakawa, and H. Murakami, “Analysis and control of a Stewart platform as base motion compensators - Part I: Kinematics using moving frames,” Nonlinear Dyn, vol. 107, no. 1, pp. 51–76, Jan. 2022, doi: 10.1007/s11071-021-06767-8.

[5] T. Ono, R. Eto, J. Yamakawa, and H. Murakami, “Analysis and control of a Stewart platform as base motion compensators—part II: dynamics,” Nonlinear Dyn, vol. 106, no. 4, pp. 3161–3182, Dec. 2021, doi: 10.1007/s11071-021-06749-w.

[6] L. Liang, Z. Le, S. Zhang, and J. Li, “Modeling and controller design of an active motion compensated gangway based on inverse dynamics in joint space,” Ocean Engineering, vol. 197, Feb. 2020, doi: 10.1016/j.oceaneng.2019.106864.

[7] A. Niu, S. Wang, Y. Sun, J. Qiu, W. Qiu, and H. Chen, “Dynamic modeling and analysis of a novel offshore gangway with 3UPU/UP-RRP series-parallel hybrid structure,” Ocean Engineering, vol. 266, Dec. 2022, doi: 10.1016/j.oceaneng.2022.113122.

[8] B. Lu, Y. Fang, J. Lin, Y. Hao, and H. Cao, “Nonlinear antiswing control for offshore boom cranes subject to ship roll and heave disturbances,” Autom Constr, vol. 131, Nov. 2021, doi: 10.1016/j.autcon.2021.103843.

[9] Y. Cai, S. Zheng, W. Liu, Z. Qu, and J. Han, “Model analysis and modified control method of ship-mounted Stewart platforms for wave compensation,” IEEE Access, vol. 9, pp. 4505–4517, 2021, doi: 10.1109/ACCESS.2020.3047063.

[10] Q. Zhang, B. Tan, B. P. Gu, and X. Hu, “Docking ship heave compensation system for loading operations based on a DDPG and PID hybrid control method using a judge network,” Ocean Engineering, vol. 305, Aug. 2024, doi: 10.1016/j.oceaneng.2024.117727.

[11] Y. Wang, Y. Wei, W. Gao, T. Ma, and Y. Han, “Ocean Wave Active Compensation Analysis for Redundant Hybrid Boarding System: A Multi-Task Motion Planning Method,” J Mar Sci Eng, vol. 11, no. 4, Apr. 2023, doi: 10.3390/jmse11040708.

[12] W. Chen et al., “An ADRC-based triple-loop control strategy of ship-mounted Stewart platform for six-DOF wave compensation,” Mech Mach Theory, vol. 184, Jun. 2023, doi: 10.1016/j.mechmachtheory.2023.105289.

[13] Z. Du, X. Chen, Q. Zhang, and Y. Yang, “An extended state observer-based sliding mode control method for hydraulic servo system of marine stabilized platforms,” Ocean Engineering, vol. 279, Jul. 2023, doi: 10.1016/j.oceaneng.2023.114386.

[14] D. Silva, J. Garrido, and E. Riveiro, “Stewart Platform Motion Control Automation with Industrial Resources to Perform Cycloidal and Oceanic Wave Trajectories,” Machines, vol. 10, no. 8, Aug. 2022, doi: 10.3390/machines10080711.

[15] D. C. Vu, T. L. Nguyen, and D. H. Nguyen, “A novel approach of Consensus-based Finite-time Distributed Sliding Mode Control for Stewart platform manipulators motion tracking,” Results in Engineering, vol. 25, Mar. 2025, doi: 10.1016/j.rineng.2024.103872.

[16] T. S. Tamir, G. Xiong, Y. Tian and G. Xiong, "Passivity Based Control Of Stewart Platform For Trajectory Tracking," 2019 14th IEEE Conference on Industrial Electronics and Applications (ICIEA), Xi'an, China, 2019, pp. 988-993, doi: 10.1109/ICIEA.2019.8833935

[17] J. Lin, J. Lian, G. Zhao, H. Li, and C. Xu, “A 2-DOF drag-free control ground simulation system based on Stewart platform,” ISA Trans, vol. 146, pp. 528–540, Mar. 2024, doi: 10.1016/j.isatra.2024.01.010.

[18] B. Andrievsky, N. V. Kuznetsov, E. V. Kudryashova, O. A. Kuznetsova, and I. Zaitceva, “Signal-parametric discrete-time adaptive controller for pneumatically actuated Stewart platform,” Control Eng Pract, vol. 138, Sep. 2023, doi: 10.1016/j.conengprac.2023.105616.

[19] M. Barghandan, A. A. Pirmohamadi, S. Mobayen, and A. Fekih, “Optimal adaptive barrier-function super-twisting nonlinear global sliding mode scheme for trajectory tracking of parallel robots,” Heliyon, vol. 9, no. 2, Feb. 2023, doi: 10.1016/j.heliyon.2023.e13378.

[20] T. S. Tamir et al., “Design and Optimization of a Control Framework for Robot Assisted Additive Manufacturing Based on the Stewart Platform,” Int J Control Autom Syst, vol. 20, no. 3, pp. 968–982, Mar. 2022, doi: 10.1007/s12555-021-0058-4.

[21] A. Şumnu, İ. H. Güzelbey, and M. V. Çakir, “Simulation and PID control of a Stewart platform with linear motor,” Journal of Mechanical Science and Technology, vol. 31, no. 1, pp. 345–356, Jan. 2017, doi: 10.1007/s12206-016-1238-7.

[22] J. Velasco, Ó. Barambones, I. Calvo, P. Venegas, and C. M. Napole, “Validation of a Stewart platform inspection system with an artificial neural network controller,” Precis Eng, vol. 74, pp. 369–381, Mar. 2022, doi: 10.1016/j.precisioneng.2022.01.002.

[23] B. An et al., “Optimization of fracture reduction robot controller based on improved sparrow algorithm,” Biomimetic Intelligence and Robotics, vol. 3, no. 4, Dec. 2023, doi: 10.1016/j.birob.2023.100120.

[24] C. C. Nguyen, Z. . -L. Zhou, S. S. Antrazi and C. E. Campbell, "Efficient computation of forward kinematics and Jacobian matrix of a Stewart platform-based manipulator," IEEE Proceedings of the SOUTHEASTCON '91, Williamsburg, VA, USA, 1991, pp. 869-874 vol.2, doi: 10.1109/SECON.1991.147884

[25] K. Harib and K. Srinivasan, “Kinematic and dynamic analysis of Stewart platform-based machine tool structures,” Robotica, vol. 21, no. 5, pp. 541–554, Sep. 2003, doi: 10.1017/S0263574703005046.

[26] S. Mirjalili, A. H. Gandomi, S. Z. Mirjalili, S. Saremi, H. Faris, and S. M. Mirjalili, “Salp Swarm Algorithm: A bio-inspired optimizer for engineering design problems,” Advances in Engineering Software, vol. 114, pp. 163–191, Dec. 2017, doi: 10.1016/j.advengsoft.2017.07.002.